Letter | Editors' Suggestion

Fractional chiral hinge insulator

Anna Hackenbroich,[1,2] Ana Hudomal,[3,4] Norbert Schuch,[1,2,5,6] B. Andrei Bernevig,[7] and Nicolas Regnault[7,8]

[1]*Max-Planck-Institute of Quantum Optics, Hans-Kopfermann-Straße 1, 85748 Garching, Germany*
[2]*Munich Center for Quantum Science and Technology, Schellingstraße 4, 80799 München, Germany*
[3]*Institute of Physics Belgrade, University of Belgrade, 11080 Belgrade, Serbia*
[4]*School of Physics and Astronomy, University of Leeds, Leeds LS2 9JT, United Kingdom*
[5]*Faculty of Physics, University of Vienna, Boltzmanngasse 5, 1090 Wien, Austria*
[6]*Faculty of Mathematics, University of Vienna, Oskar-Morgenstern-Platz 1, 1090 Vienna, Austria*
[7]*Joseph Henry Laboratories and Department of Physics, Princeton University, Princeton, New Jersey 08544, USA*
[8]*Laboratoire de Physique de l'Ecole normale supérieure, ENS, Université PSL, CNRS, Sorbonne Université, Université Paris-Diderot, Sorbonne Paris Cité, Paris 75005, France*

(Received 26 October 2020; accepted 2 April 2021; published 23 April 2021)

We propose and study a wave function describing an interacting three-dimensional fractional chiral hinge insulator (FCHI) constructed by Gutzwiller projection of two noninteracting second-order topological insulators with chiral hinge modes at half filling. We use large-scale variational Monte Carlo computations to characterize the model states via the entanglement entropy and charge-spin fluctuations. We show that the FCHI possesses fractional chiral hinge modes characterized by a central charge $c = 1$ and Luttinger parameter $K = 1/2$, like the edge modes of a Laughlin $1/2$ state. The bulk and surface topology is characterized by the topological entanglement entropy (TEE) correction to the area law. While our computations indicate a vanishing bulk TEE, we show that the gapped surfaces host an unconventional two-dimensional topological phase. In a clear departure from the physics of a Laughlin $1/2$ state, we find a TEE per surface compatible with $(\ln\sqrt{2})/2$, half that of a Laughlin $1/2$ state. This value cannot be obtained from topological quantum field theory for purely two-dimensional systems. For the sake of completeness, we also investigate the topological degeneracy.

DOI: 10.1103/PhysRevB.103.L161110

I. INTRODUCTION

Strong interactions in condensed-matter systems can lead to fascinating emergent phenomena. In two-dimensional (2D) systems, strong interactions may lead to the emergence of topological order (TO), such as that experimentally observed in the fractional quantum Hall effect. Features of TO in two dimensions include a nontrivial ground state degeneracy on certain surfaces and the appearance of itinerant excitations with fractional quantum numbers and braiding statistics. It has long been an active field of study to extend this rich physics to three-dimensional (3D) strongly interacting systems, where the emergent physics can be even more diverse, including systems with fractonic excitations [1,2]. Whereas many microscopic models based on interacting spin systems have been proposed to exhibit TO in three dimensions, such as the 3D toric code [3] and 3D Kitaev models [4–7], and there are treatments of 3D fractional topological insulators using effective field theory [8,9], there is a scarcity of electronic or realistic examples that could be experimentally relevant.

Among the 3D electronic topological insulators (TIs), an entirely new class was recently discovered: Certain TIs protected by crystalline symmetries, now dubbed higher-order TIs [10–25], possess a much richer bulk-boundary correspondence than conventional, or first-order, TIs. For example, a 3D chiral hinge insulator (CHI) exists whose gapped surfaces are connected by gapless chiral hinge modes [12]. Higher-order TIs in two and three dimensions have been experimentally observed in materials [26], mechanical [27], acoustic [28,29], photonic [30–33], and electrical [34,35,38] systems. Two-dimensional higher-order TIs have also been studied in the strongly interacting regime [36,37].

In this Letter, we provide a first stepping stone in the realization of a full-fledged electronic 3D fractional TI by building a 3D fractional chiral hinge insulator (FCHI) model wave function. Indeed, the hinge modes of the noninteracting CHI are of the same nature as the edge modes of a Chern insulator, two copies of which at fractional filling and with strong interactions form a fractional Chern insulator (FCI) hosting fractional quantum Hall physics [39–41]. Therefore, we may speculate that under similar conditions the FCHI will also display nontrivial topology with fractionalized excitations at least at the hinges or surfaces.

Numerical computations and especially exact diagonalizations for interacting electronic systems in three dimensions are notoriously difficult due to the spatial dimensionality. To partially circumvent this challenge, we will rely on a model wave function, a fruitful approach for TO, to capture the FCHI. This approach has been extensively applied in the realm of the fractional quantum Hall effect [42,43] and FCIs [44]. In order to define the FCHI wave function, we will make use of Gutzwiller projection, a systematic method to construct interacting model wave functions starting from copies of noninteracting ground states. Large-scale variational Monte Carlo

(MC) simulations then allow us to analyze this wave function for bigger system sizes than possible with other methods.

To probe the topological content of the wave function, we will study the entanglement entropy (EE), which can be evaluated in MC simulations [44–48] and follows an area law with characteristic subleading corrections [49]. In two dimensions there are logarithmic corrections for gapless edge modes [50–52] which along with the constant topological entanglement entropy (TEE) correction to the bulk area law [53,54] provide information on the system's topology. In three dimensions, corrections to the bulk area law include the TEE and possible size-dependent corrections for fractonic systems and layered constructions [55–57]. In particular, we study the hinge modes in an open system and show that they are fractionalized excitations characterized by a central charge $c = 1$ and Luttinger parameter $K = 1/2$, like the FCI edge modes. Next, we study the TEE of the bulk system and that of the gapped surfaces. Whereas our computations indicate a vanishing bulk TEE, we show that the gapped surfaces host a nontrivial two-dimensional topological phase with a TEE per surface compatible with half that of a Laughlin 1/2 state. For completeness, we then study the linear independence of different interacting wave functions obtained by changing the boundary conditions for the underlying fermions.

II. MODEL WAVE FUNCTION

We consider an interacting model wave function obtained by Gutzwiller projection of the ground state of a noninteracting 3D second-order TI with chiral hinge modes. The CHI model is described by a local Hamiltonian for spinless fermions with four sites per unit cell [12] [see Fig. 1(a) for a sketch of the model]. The ground state $|\psi\rangle$ of the CHI model lies at filling $\nu = 1/2$ of the lattice. With open boundary conditions (OBC) in the x and y directions, each of the four hinges of the CHI parallel to the z axis supports a single chiral mode localized at the hinge. Each hinge mode corresponds to a free bosonic mode with central charge $c = 1$ and Luttinger parameter $K = 1$ akin to the edge modes of a Chern insulator [58]. Since the CHI model is noninteracting, it does not have TO or a nontrivial ground state degeneracy with periodic boundary conditions (PBC).

In order to define the interacting model wave function $|\Psi\rangle$, we take two copies $|\psi_s\rangle$ of the ground state of the CHI model at half filling, to which we assign different values $s \in \{\uparrow, \downarrow\}$ of a spinlike degree of freedom. The interacting wave function is obtained as the Gutzwiller projection

$$|\Psi\rangle = P_G[|\psi_\uparrow\rangle \otimes |\psi_\downarrow\rangle] \tag{1}$$

of the product of the two noninteracting wave functions. With $\hat{n}_{s,i}$ denoting the particle number operator for fermions of spin s on the lattice site i, the Gutzwiller projection operator is expressed as

$$P_G = \prod_i (1 - \hat{n}_{\uparrow,i}\hat{n}_{\downarrow,i}). \tag{2}$$

It forbids simultaneous occupancy of any lattice site i by both a particle with spin $\uparrow$ and a particle with spin $\downarrow$. Therefore, it simulates the effect of a very large on-site Hubbard interaction. Since each copy of the ground state of the CHI model has a filling $\nu_{\psi_\uparrow} = \nu_{\psi_\downarrow} = 1/2$, the Gutzwiller projection enforces that the interacting wave function lies at filling $\nu_\Psi = 1/2$ with exactly one particle per lattice site (each lattice site having a spin degree of freedom which can take two values). Hence, charge fluctuations are completely frozen, and the only relevant degree of freedom in the interacting wave function is the spin s.

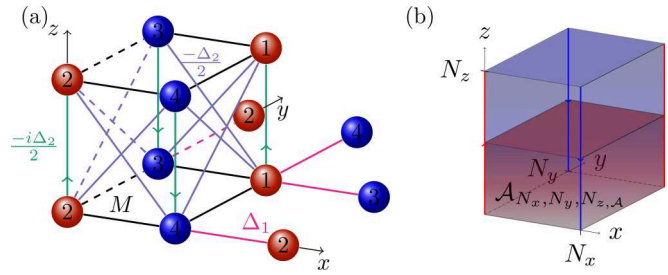

FIG. 1. (a) Local real-space model for a 3D second-order TI with chiral hinge states. The Hamiltonian is defined on a cubic lattice with a unit cell of four sites lying in the xy plane. In this plane, sites in the same unit cell are connected by a nearest-neighbor hopping M marked by black lines ($-M$ for dashed black lines). In the xy plane, sites in adjacent unit cells are connected by a nearest-neighbor hopping Δ_1 marked by violet lines ($-\Delta_1$ for dashed violet lines). In the z direction, adjacent unit cells are connected by a real next-nearest-neighbor hopping $-\Delta_2/2$ marked by light blue lines ($\Delta_2/2$ for dashed light blue lines). In addition, there is a purely imaginary nearest-neighbor hopping between adjacent unit cells in the z direction with a value of $-i\Delta_2/2$ in the direction of the green arrows. We study the model for parameter values $M = \Delta_1 = \Delta_2 = 1$, where the correlation length is close to its minimal value [58]. (b) Three-dimensional system with OBC and N_x, N_y unit cells in the x, y directions and periodic boundaries and N_z sites in the z direction. The subsystem $\mathcal{A}_{N_x,N_y,N_{z,\mathcal{A}}}$ consists of N_x, N_y unit cells in the x, y directions and $N_{z,\mathcal{A}}$ unit cells in the z direction.

III. CHARACTERIZATION OF HINGE MODES

With OBC in the x and y directions, the interacting model wave function $|\Psi\rangle$ is expected to possess one gapless chiral mode at each of the four hinges parallel to the z axis, inherited from the hinge modes of the noninteracting CHI. Like the edge modes of chiral topologically ordered phases in two dimensions, we expect the hinge modes of $|\Psi\rangle$ to be described by a chiral conformal field theory (CFT). Moreover, since $|\Psi\rangle$ is interacting, we expect its hinge CFT to be possibly different from the trivial free-boson CFT describing the hinge modes of the noninteracting CHI.

In order to characterize the chiral hinge modes, we adapt the methods that were previously employed for 2D chiral phases [51,52,59] to the 3D setting: We study the second Rényi entropy $S^{(2)}$ and spin fluctuations of $|\Psi\rangle$, in focusing on the critical contributions stemming from the *physical* hinges. We evaluate these observables for the interacting wave function $|\Psi\rangle$ in large-scale MC simulations using the SWAP-operator technique [60] with sign-problem refinement [58,61].

We consider the geometry sketched in Fig. 1(b): a total system with $N_x \times N_y \times N_z$ unit cells, OBC in the xy plane, and PBC in the z direction to ensure that the only gapless excitations are the four hinge states. We consider a series of

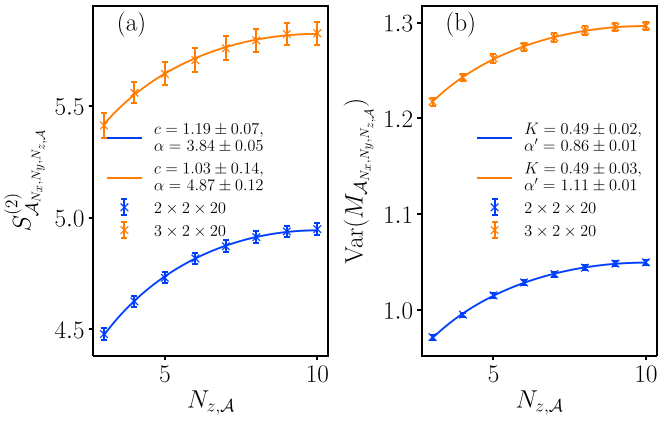

FIG. 2. Second Rényi entropy and spin fluctuations of the interacting model wave function $|\Psi\rangle$ for a series of subsystems $\mathcal{A}_{N_x,N_y,N_{z,\mathcal{A}}}$ [58]. We plot MC data obtained for two different systems sizes $2 \times 2 \times 20$ (in blue) and $3 \times 2 \times 20$ (in orange). (a) Scaling of the second Rényi entropy, fit to the prediction of Eq. (3). (b) Scaling of the spin fluctuations, fit to the prediction of Eq. (6).

subsystems $\mathcal{A}_{N_x,N_y,N_{z,\mathcal{A}}}$ with N_x, N_y unit cells in the x, y directions and $N_{z,\mathcal{A}} \in \{1, \ldots, N_z - 1\}$ unit cells in the z direction, marked in red in Fig. 1(b). $\mathcal{A}_{N_x,N_y,N_{z,\mathcal{A}}}$ bisect each of four physical hinge modes into a part of length $N_{z,\mathcal{A}}$ contained in $\mathcal{A}_{N_x,N_y,N_{z,\mathcal{A}}}$ and the remaining part outside of the subsystem. Hence, we expect that the EE and spin fluctuations with respect to $\mathcal{A}_{N_x,N_y,N_{z,\mathcal{A}}}$ will contain signatures from the hinges.

Specifically, if the hinge modes are described by a chiral CFT with central charge c, the second Rényi entropy $S^{(2)}$ of $|\Psi\rangle$ with respect to $\mathcal{A}_{N_x,N_y,N_{z,\mathcal{A}}}$ for different $N_{z,\mathcal{A}}$ at fixed N_x and N_y is expected to scale as

$$S^{(2)}_{\mathcal{A}_{N_x,N_y,N_{z,\mathcal{A}}}}(N_{z,\mathcal{A}}) = \alpha + 4 \times S^{(2)}_{\mathrm{crit}}(N_{z,\mathcal{A}}; N_z). \tag{3}$$

Here, α is a constant independent of $N_{z,\mathcal{A}}$. It includes the area law contributions from the virtual surfaces at $z = 0, N_{z,\mathcal{A}}$ which scale proportional to $N_x N_y$ and are therefore independent of $N_{z,\mathcal{A}}$ in the thermodynamic limit, and any potential corner contributions. In Eq. (3),

$$S^{(2)}_{\mathrm{crit}}(N_{z,\mathcal{A}}; N_z) = \frac{c}{8} \ln\left[\frac{N_z}{\pi} \sin\left(\frac{\pi N_{z,\mathcal{A}}}{N_z}\right)\right] \tag{4}$$

is the second Rényi entropy of a periodic one-dimensional chiral critical mode with central charge c and total system size N_z restricted to a single interval of length $N_{z,\mathcal{A}}$ [50]. The factor of 4 in Eq. (3) takes into account the four hinge modes, which contribute equally to the EE.

The scaling of the second Rényi entropy of $|\Psi\rangle$ as computed from MC is shown in Fig. 2(a) for two different system sizes, $2 \times 2 \times 20$ and $3 \times 2 \times 20$. For computational reasons, we choose N_x and N_y to be much smaller than N_z [58]. Due to the short correlation length of the CHI, equal to one lattice spacing [58], we may expect that the characteristic parameters approach their thermodynamic limit even for small N_x, N_y. The logarithmic scaling from the hinge states is clearly visible, and numerical values for c and α can be extracted by fitting the data to Eq. (3). The numerical value for the central charge is $c = 1.19 \pm 0.07$ for $2 \times 2 \times 20$ and $c = 1.03 \pm 0.14$ for $3 \times 2 \times 20$. This provides strong evidence that the hinge modes of the interacting model wave function $|\Psi\rangle$ are described by a chiral free-boson CFT with central charge $c = 1$.

Free-boson CFTs with $c = 1$ are characterized by their Luttinger parameter K. For such Luttinger liquids, the variance of the U(1) current integrated over a subsystem scales proportionally to the EE, where the proportionality constant allows the extraction of K [59]. Since charge fluctuations are completely frozen in the wave function $|\Psi\rangle$, the relevant U(1) symmetry stems from the spin degree of freedom, and we need to consider the fluctuations of the number $M_{\mathcal{A}}$ of particles with spin $\uparrow$ in a subsystem $\mathcal{A}$. Concretely, we consider the variance

$$\mathrm{Var}\left(M_{\mathcal{A}_{N_x,N_y,N_{z,\mathcal{A}}}}\right) \equiv \left\langle M^2_{\mathcal{A}_{N_x,N_y,N_{z,\mathcal{A}}}}\right\rangle - \left\langle M_{\mathcal{A}_{N_x,N_y,N_{z,\mathcal{A}}}}\right\rangle^2, \tag{5}$$

which is expected to scale as [59]

$$\mathrm{Var}\left(M_{\mathcal{A}_{N_x,N_y,N_{z,\mathcal{A}}}}\right) = 2\frac{K}{\pi^2} \ln\left[\frac{N_z}{\pi} \sin\left(\frac{\pi N_{z,\mathcal{A}}}{N_z}\right)\right] + \alpha' \tag{6}$$

with the Luttinger parameter K and a constant α' independent of $N_{z,\mathcal{A}}$.

The scaling of the spin fluctuations in the wave function $|\Psi\rangle$ as computed from MC is shown in Fig. 2(b) for two different system sizes, $2 \times 2 \times 20$ and $3 \times 2 \times 20$. Remarkably, even for these small sizes, the numerical value for K extracted by fitting the data to Eq. (6) is $K = 0.49 \pm 0.02$ for $2 \times 2 \times 20$ and $K = 0.49 \pm 0.03$ for $3 \times 2 \times 20$. This provides strong evidence that the Luttinger parameter for the chiral hinge modes of the interacting higher-order TI is $K = 1/2$, similar to the edge modes of a FCI.

IV. TOPOLOGICAL DEGENERACY AND TOPOLOGICAL ENTANGLEMENT ENTROPY

In two dimensions, fractionalized excitations such as those of the edge modes of an FCI are an indication of bulk TO. Above, we showed that the FCHI has fractional hinge modes. It is therefore natural to investigate whether it also possesses nontrivial topology in the bulk and on the surfaces. Two-dimensional topologically ordered systems are characterized by a nonzero TEE and a nontrivial topological degeneracy on surfaces with a genus greater than zero. In three dimensions, TEE and topological degeneracy remain important signatures of nontrivial topology. We now study these signatures for the FCHI model.

a. Topological entanglement entropy. In order to compute the TEE of the FCHI, we use the Kitaev-Preskill construction [53] extended to 3D systems [55]. As sketched in Fig. 3(a), the system is divided into four regions, $\mathcal{A}$, $\mathcal{B}$, $\mathcal{C}$, and $\mathcal{D}$, which are translation invariant in the z direction and whose cross sections with the xy plane form the pattern required for the usual 2D Kitaev-Preskill cut. The EE of these regions and their unions can be collected into the linear combination

$$-\gamma = S^{(2)}_{\mathcal{ABC}} - S^{(2)}_{\mathcal{AB}} - S^{(2)}_{\mathcal{BC}} - S^{(2)}_{\mathcal{AC}} + S^{(2)}_{\mathcal{A}} + S^{(2)}_{\mathcal{B}} + S^{(2)}_{\mathcal{C}}, \tag{7}$$

which cancels all contributions from the virtual surfaces and hinges. The remaining quantity, denoted γ, could contain two contributions, $\gamma = \gamma_{3D} + N_z \gamma_{2D}$. The constant γ_{3D} is the 3D TEE [55]. $\gamma_{2D} N_z$ would occur for layered constructions of 2D

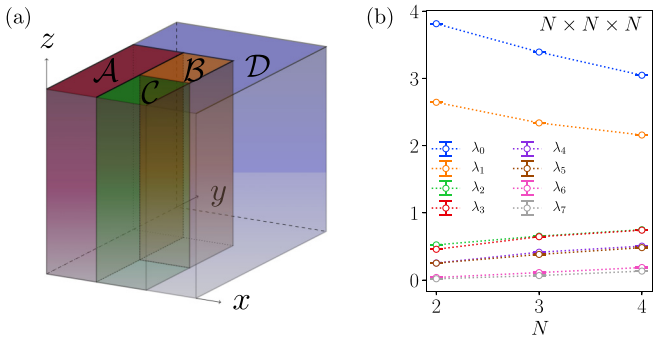

FIG. 3. (a) Subsystems $\mathcal{A}$, $\mathcal{B}$, $\mathcal{C}$, and $\mathcal{D}$ for the extraction of the bulk TEE using a Kitaev-Preskill cut. Note that the subsystems are translation invariant in the z direction. (b) Scaling of the eigenvalues λ_i with $i = 0, \ldots, 7$ of the overlap matrix $\mathcal{O}$ of the FCHI on the isotropic three-torus with $N \times N \times N$ unit cells.

topological orders perpendicular to the z direction with 2D TEE γ_{2D} [55] or in some fractonic systems [1,2].

We have computed γ for the FCHI on the three-torus in large-scale variational MC computations. For the geometry sketched in Fig. 3(a), we were able to study the FCHI with $3 \times 3 \times 2$ unit cells, for which we found $\gamma = -0.08 \pm 0.04$, and with $3 \times 3 \times 3$ unit cells, for which we found $\gamma = -0.06 \pm 0.11$. In both cases, the subsystem $\mathcal{A}$ is of size $1 \times 2 \times N_z$ unit cells, and the subsystems $\mathcal{B}$ and $\mathcal{C}$ are of size $1 \times 1 \times N_z$ unit cells [62]. Because of the intrinsic anisotropy of the FCHI, we also considered a second geometry obtained by rotating the subsystems in Fig. 3(a) along the y axis such that they are translation invariant in the x direction while leaving the insulator unchanged. Here, we computed γ for a system of $2 \times 3 \times 5$ unit cells [63] and found $\gamma = -0.009 \pm 0.102$. All these values are consistent with $\gamma = 0$ (up to small finite-size effects for $3 \times 3 \times 2$) *irrespective* of the orientation of the cut. We stress that γ is several orders of magnitude smaller than any of the EEs appearing in Eq. (7), excluding the existence of both a nonvanishing 3D TEE γ_{3D} and a nonzero γ_{2D}.

Since we have not been able to find any clear signature of a true nontrivial bulk topology, we now probe the nature of the gapped surfaces perpendicular to the x direction [64]. Since the vertical hinges host fractionalized one-dimensional modes like those of an FCI, we may speculate that the vertical surfaces host some nontrivial TO [65]. To characterize it, we compute γ according to Eq. (7) for the geometry obtained by rotating the subsystems in Fig. 3(a) as described above, OBC in the x direction, and PBC in the y and z directions. We have performed this computation for a system with $2 \times 3 \times 5$ unit cells and found $\gamma = 0.31 \pm 0.16$ [66]. Since the same computation with PBC in x yields a vanishing result for γ as discussed above, this nonzero value is due entirely to the two surfaces at $x = 0$ and $x = N_x - 1$ and confirms that the vertical surfaces host a nontrivial 2D TO. Indeed, each surface contributes with $\gamma^{2D}_{\mathrm{FCHI}} = \gamma/2$ to the TEE. The value of $\gamma^{2D}_{\mathrm{FCHI}}$ is consistent with $(\ln\sqrt{2})/2$, a clear departure from the TEE of a single 2D FCI in the Laughlin $1/2$ phase.

b. Topological degeneracy. In order to study the topological degeneracy of the FCHI we closely follow a well-known approach established for 2D projected wave functions such as the FCI. On the 2D torus, one defines four interacting wave functions by choosing PBC or antiperiodic boundary conditions (APBC) for the underlying fermions in each direction of the torus. For the FCI, these four states yield two linearly independent wave functions, as expected in the phase of the Laughlin wave function with filling $\nu = 1/2$ [58].

For the FCHI, we consider eight independent ansatz states on the 3D torus obtained by Gutzwiller projection of the noninteracting CHI wave function with PBC or APBC in each direction. The ground state degeneracy is then given by the rank of an eight-dimensional overlap matrix $\mathcal{O}$ containing the normalized overlaps of these ansatz states [58]. Note that the topological degeneracy could, in principle, be larger than 8. In such a case, the rank of the overlap matrix considered here would still be, at most, 8, and our approach would fail to measure the full ground state degeneracy.

We have studied the topological degeneracy of the FCHI on isotropic three-tori with $N \times N \times N$ unit cells up to $N = 4$ using variational MC simulations [58]. The results are shown in Fig. 3(b). For these system sizes, we observe a separation of the eigenvalues of the overlap matrix $\mathcal{O}$ into a group of two larger eigenvalues and a group of six smaller eigenvalues. However, there is no clear trend indicating that the former would converge to a finite value and the latter to zero in the thermodynamic limit. The finite-size effects due to the numerical limitation to small system sizes therefore do not allow us to draw clear conclusions about the asymptotic topological degeneracy from these results.

Since we have observed a nontrivial surface topology from the TEE, we want to investigate whether these modes contribute a topological degeneracy. For that purpose, we have also studied the degeneracy of the FCHI with OBC in the x direction, meaning each surface mode is defined on a 2D torus. In this geometry, four ansatz states are generated by changing the boundary conditions for the underlying CHI in the two periodic directions. We have found behavior very similar to the full-PBC case, namely, two larger eigenvalues but no clear evidence of a reduction of the bulk degeneracy in the thermodynamic limit [58]. Finally, we mention that we have also analyzed the topological degeneracy for very anisotropic three-tori with N_z much larger than $N_x = N_y$. An extensive discussion is given in the Supplemental Material [58].

V. DISCUSSION AND CONCLUSION

We have studied a model wave function for a 3D chiral hinge insulator with strong interactions at fractional band filling using extensive MC simulations. By studying the EE and spin fluctuations in an open geometry, we showed that the hinges host fractional gapless modes which have the same characterization as the edge modes of an FCI in the Laughlin $1/2$ phase. We have also studied the system's topology through the topological degeneracy and the TEE. While the results for the topological degeneracy remain inconclusive due to the small number of numerically accessible system sizes, our results point to the absence of a bulk TEE. However, we found clear signatures of a nontrivial 2D topological order on the vertical surfaces. Interestingly, the TEE contribution per surface is consistent with $\gamma^{2D}_{\mathrm{FCHI}} = (\ln\sqrt{2})/2$, in other words

half of the TEE of an FCI. This result cannot be explained using a quantum dimension since a TEE of $(\ln\sqrt{2})/2$ would correspond to a total quantum dimension $2^{1/4}$, whereas any nontrivial total quantum dimension has to be larger than or equal to $\sqrt{2}$. This suggests the emergence of a highly unconventional surface topology *that cannot be realized in a strictly 2D system*, with a nontrivial relation to the hinge modes [65]. In this Letter, we have restricted our analysis to the gapped surfaces and their gapless edges. It would be highly interesting, but very numerically challenging, to consider the top and bottom surfaces, which host single Dirac cones in the noninteracting CHI. Their fate in the interacting system is yet unknown and beyond the scope of the present work, but it should be the focus of further study.

ACKNOWLEDGMENTS

We thank B. Estienne for enlightening discussions. A. Hackenbroich and N.S. acknowledge support from the European Research Council (ERC) under the European Union's Horizon 2020 research and innovation program through the ERC Starting Grant WASCOSYS (Grant No. 636201) and the ERC Consolidator Grant SEQUAM (Grant No. 863476) and from the Deutsche Forschungsgemeinschaft (DFG) under Germany's Excellence Strategy (EXC-2111-390814868). A. Hackenbroich and N.R. were supported by Grant No. ANR-17-CE30-0013-01. N.R. was partially supported by NSF through Princeton University's Materials Research Science and Engineering Center (Grant No. DMR-2011750B). A. Hudomal acknowledges funding provided by the Institute of Physics Belgrade, through the grant from the Ministry of Education, Science, and Technological Development of the Republic of Serbia, as well as by the Science Fund of the Republic of Serbia, under the Key2SM project (PROMIS program, Grant No. 6066160). Part of the numerical simulations were performed at the PARADOX-IV supercomputing facility at the Scientific Computing Laboratory, National Center of Excellence for the Study of Complex Systems, Institute of Physics Belgrade. B.A.B. was supported by DOE Grant No. DE-SC0016239, the Schmidt Fund for Innovative Research, Simons Investigator Grant No. 404513, the Packard Foundation, NSF-EAGER Grant No. DMR 1643312, NSF-MRSEC Grants No. DMR-1420541 and DMR-2011750, ONR Grant No. N00014-20-1-2303, the Gordon and Betty Moore Foundation through Grant No. GBMF8685 towards the Princeton theory program, U.S-Israel Binational Science Foundation Grant No. 2018226, and the Princeton Global Network Funds.

[1] R. M. Nandkishore and M. Hermele, Annu. Rev. Condens. Matter Phys. **10**, 295 (2019).
[2] M. Pretko, X. Chen, and Y. You, Int. J. Mod. Phys. A **35**, 2030003 (2020).
[3] C. Castelnovo and C. Chamon, Phys. Rev. B **78**, 155120 (2008).
[4] S. Ryu, Phys. Rev. B **79**, 075124 (2009).
[5] I. Mondragon-Shem and T. L. Hughes, J. Stat. Mech. (2014) P10022.
[6] S. Mandal and N. Surendran, Phys. Rev. B **79**, 024426 (2009).
[7] N. C. Randeep and N. Surendran, Phys. Rev. B **98**, 125136 (2018).
[8] J. Maciejko, X.-L. Qi, A. Karch, and S.-C. Zhang, Phys. Rev. Lett. **105**, 246809 (2010).
[9] B. Swingle, M. Barkeshli, J. McGreevy, and T. Senthil, Phys. Rev. B **83**, 195139 (2011).
[10] W. A. Benalcazar, B. A. Bernevig, and T. L. Hughes, Science **357**, 61 (2017).
[11] W. A. Benalcazar, B. A. Bernevig, and T. L. Hughes, Phys. Rev. B **96**, 245115 (2017).
[12] F. Schindler, A. M. Cook, M. G. Vergniory, Z. Wang, S. S. Parkin, B. A. Bernevig, and T. Neupert, Sci. Adv. **4**, eaat0346 (2018).
[13] Z. Song, Z. Fang, and C. Fang, Phys. Rev. Lett. **119**, 246402 (2017).
[14] J. Langbehn, Y. Peng, L. Trifunovic, F. von Oppen, and P. W. Brouwer, Phys. Rev. Lett. **119**, 246401 (2017).
[15] S. Parameswaran and Y. Wan, Physics **10**, 132 (2017).
[16] E. Khalaf, Phys. Rev. B **97**, 205136 (2018).
[17] M. Geier, L. Trifunovic, M. Hoskam, and P. W. Brouwer, Phys. Rev. B **97**, 205135 (2018).
[18] L. Trifunovic and P. W. Brouwer, Phys. Rev. X **9**, 011012 (2019).
[19] Y. You, T. Devakul, F. J. Burnell, and T. Neupert, Phys. Rev. B **98**, 235102 (2018).
[20] A. Rasmussen and Y.-M. Lu, Phys. Rev. B **101**, 085137 (2020).
[21] S. A. A. Ghorashi, X. Hu, T. L. Hughes, and E. Rossi, Phys. Rev. B **100**, 020509(R) (2019).
[22] O. Dubinkin and T. L. Hughes, Phys. Rev. B **99**, 235132 (2019).
[23] Y. X. Zhao, Y. Lu, and S. A. Yang, arXiv:2005.14500.
[24] Y. You, J. Bibo, and F. Pollmann, Phys. Rev. Research **2**, 033192 (2020).
[25] B. Kang, W. Lee, and G. Y. Cho, Phys. Rev. Lett. **126**, 016402 (2021).
[26] F. Schindler, Z. Wang, M. G. Vergniory, A. M. Cook, A. Murani, S. Sengupta, A. Y. Kasumov, R. Deblock, S. Jeon, I. Drozdov, H. Bouchiat, S. Guéron, A. Yazdani, B. A. Bernevig, and T. Neupert, Nat. Phys. **14**, 918 (2018).
[27] M. Serra-Garcia, V. Peri, R. Süsstrunk, O. R. Bilal, T. Larsen, L. G. Villanueva, and S. D. Huber, Nature (London) **555**, 342 (2018).
[28] H. Xue, Y. Yang, F. Gao, Y. Chong, and B. Zhang, Nat. Mater. **18**, 108 (2019).
[29] X. Ni, M. Weiner, A. Alú, and A. B. Khanikaev, Nat. Mater. **18**, 113 (2019).
[30] S. Mittal, V. V. Orre, G. Zhu, M. A. Gorlach, A. Poddubny, and M. Hafezi, Nat. Photon. **13**, 692 (2019).
[31] A. E. Hassan, F. K. Kunst, A. Moritz, G. Andler, E. J. Bergholtz, and M. Bourennane, Nat. Photon. **13**, 697 (2019).
[32] B.-Y. Xie, G.-X. Su, H.-F. Wang, H. Su, X.-P. Shen, P. Zhan, M.-H. Lu, Z.-L. Wang, and Y.-F. Chen, Phys. Rev. Lett. **122**, 233903 (2019).

[33] Y. Yang, Z. Jia, Y. Wu, R.-C. Xiao, Z.-H. Hang, H. Jiang, and X. C. Xie, Sci. Bull. **65**, 531 (2020).
[34] C. W. Peterson, W. A. Benalcazar, T. L. Hughes, and G. Bahl, Nature (London) **555**, 346 (2018).
[35] S. Imhof, C. Berger, F. Bayer, J. Brehm, L. W. Molenkamp, T. Kiessling, F. Schindler, C. H. Lee, M. Greiter, T. Neupert, and R. Thomale, Nat. Phys. **14**, 925 (2018).
[36] K. Laubscher, D. Loss, and J. Klinovaja, Phys. Rev. Research **1**, 032017(R) (2019).
[37] K. Laubscher, D. Loss, and J. Klinovaja, Phys. Rev. Research **2**, 013330 (2020).
[38] M. Serra-Garcia, R. Süsstrunk, and S. D. Huber, Phys. Rev. B **99**, 020304(R) (2019).
[39] D. N. Sheng, Z.-C. Gu, K. Sun, and L. Sheng, Nat. Commun. **2**, 389 (2011).
[40] T. Neupert, L. Santos, C. Chamon, and C. Mudry, Phys. Rev. Lett. **106**, 236804 (2011).
[41] N. Regnault and B. A. Bernevig, Phys. Rev. X **1**, 021014 (2011).
[42] R. B. Laughlin, Phys. Rev. Lett. **50**, 1395 (1983).
[43] G. Moore and N. Read, Nucl. Phys. B **360**, 362 (1991).
[44] Y. Zhang and A. Vishwanath, Phys. Rev. B **87**, 161113(R) (2013).
[45] J. Shao, E.-A. Kim, F. D. M. Haldane, and E. H. Rezayi, Phys. Rev. Lett. **114**, 206402 (2015).
[46] Y. Zhang, T. Grover, and A. Vishwanath, Phys. Rev. B **84**, 075128 (2011).
[47] J. Pei, S. Han, H. Liao, and T. Li, Phys. Rev. B **88**, 125135 (2013).
[48] J. Wildeboer and N. E. Bonesteel, Phys. Rev. B **94**, 045125 (2016).
[49] M. Srednicki, Phys. Rev. Lett. **71**, 666 (1993).
[50] P. Calabrese and J. Cardy, J. Phys. A **42**, 504005 (2009).
[51] V. Crépel, N. Claussen, B. Estienne, and N. Regnault, Nat. Commun. **10**, 1861 (2019).
[52] V. Crépel, N. Claussen, N. Regnault, and B. Estienne, Nat. Commun. **10**, 1860 (2019).
[53] A. Kitaev and J. Preskill, Phys. Rev. Lett. **96**, 110404 (2006).
[54] M. Levin and X.-G. Wen, Phys. Rev. Lett. **96**, 110405 (2006).
[55] T. Grover, A. M. Turner, and A. Vishwanath, Phys. Rev. B **84**, 195120 (2011).
[56] H. Ma, A. T. Schmitz, S. A. Parameswaran, M. Hermele, and R. M. Nandkishore, Phys. Rev. B **97**, 125101 (2018).
[57] H. He, Y. Zheng, B. A. Bernevig, and N. Regnault, Phys. Rev. B **97**, 125102 (2018).
[58] See Supplemental Material at http://link.aps.org/supplemental/10.1103/PhysRevB.103.L161110 for the additional information on our numerical methods, benchmarks on a two-dimensional fractional Chern insulator and the non-interacting three-dimensional chiral hinge insulator, and additional results for the topological degeneracy of the three-dimensional model.
[59] B. Estienne and J.-M. Stéphan, Phys. Rev. B **101**, 115136 (2020).
[60] M. B. Hastings, I. González, A. B. Kallin, and R. G. Melko, Phys. Rev. Lett. **104**, 157201 (2010).
[61] Y. Zhang, T. Grover, and A. Vishwanath, Phys. Rev. Lett. **107**, 067202 (2011).
[62] We recall that the number of physical sites for these subsystems is $2 \times 4 \times N_z$ and $2 \times 2 \times N_z$, respectively.
[63] We recall that the number of physical sites in this case is $4 \times 6 \times 5$. Thus, although $N_x = 2$, the PBC along x are nontrivial. Here, subsystem $\mathcal{A}$ is of size $2 \times 2 \times 2$ unit cells, and subsystems $\mathcal{B}$ and $\mathcal{C}$ are of size $2 \times 1 \times 2$ unit cells.
[64] We could alternatively choose those perpendicular to the y direction.
[65] A. Tiwari, M.-H. Li, B. A. Bernevig, T. Neupert, and S. A. Parameswaran, Phys. Rev. Lett. **124**, 046801 (2020).
[66] Here, the statistical error bar is a conservative estimate, in particular much larger than the remaining fluctuations in the mean of the MC computations [58]. We stress that our conservative error bar confirms a nontrivial TEE smaller than $\ln\sqrt{2}$ per surface.